Influence of growth temperature on the vortex pinning properties of pulsed laser deposited $YBa_2Cu_3O_{7-x}$ thin films

Z. Chen,[1,a] F. Kametani,[1] S. I. Kim,[1] D. C. Larbalestier,[1] H. W. Jang,[2] K. J. Choi,[2] and C. B. Eom[2]
[1]*National High Magnetic Field Laboratory, Florida State University, Tallahassee, Forida 32310, USA*
[2]*Department of Materials Science and Engineering, University of Wisconsin-Madison, Madison, Wisconsin 53706, USA*

(Received 3 October 2007; accepted 22 December 2007; published online 29 February 2008)

Epitaxial high-temperature superconducting $YBa_2Cu_3O_{7-x}$ thin films grown on 2° miscut (001) $(LaAlO_3)_{0.3}$-$(SrAl_{0.5}Ta_{0.5}O_3)_{0.7}$ substrates by pulsed laser deposition show significant and systematic changes in flux pinning properties on changing the substrate temperature from 730 to 820 °C. The bulk pinning force is highest for the 760 °C growth, rising to a maximum of 4.4 GN/m^3 at 77 K, though there are indications that vortex pinning strength is even higher for the 730 °C growth once allowance for the current-blocking effects of *a*-axis oriented grains is made. Cross-sectional transmission electron microscope images show that the density of antiphase boundaries, stacking faults, and edge dislocations increases strongly with decreasing growth temperature, and is highest at 730 °C. In spite of the enhanced density of the pinning defects mentioned above, their vortex pinning effect is still much smaller than for insulating nanoparticles of high density and optimum size, where pinning forces can be four to five times higher. © *2008 American Institute of Physics*. [DOI: 10.1063/1.2885716]

I. INTRODUCTION

The critical current density J_c in thin-film $YBa_2Cu_3O_{7-x}$ (YBCO) is typically three orders of magnitude higher at 77 K than in single crystals.[1] The high J_c of films is often attributed to general growth disorder and correlated defects induced by the substrate, especially extended defects such as dislocations.[2–4] For YBCO films epitaxially grown by the pulsed laser deposition (PLD) method on single crystal substrates, e.g., $SiTiO_3$, the formation of dislocations is greatly related to island or spiral growth modes, and the density of dislocations can be enhanced by decreasing the growth temperature of YBCO.[5–7]

For electronics applications, smoother surfaces are desired, which can be obtained by step-flow growth, which occurs at higher growth temperatures or on substrates cut with a small vicinal angle.[8–10] However, step-flow growth largely suppresses the formation of extended dislocations,[8,11] making J_c values lower.[12] At lower growth temperatures, however, vicinal substrates can provide many additional defects that, for example, can produce high densities of antiphase boundaries and stacking faults that make strong-pinning centers in YBCO films.[9] Submicron sized pores[13] are another defect produced by vicinal substrates that can strongly enhance J_c (Ref. 14) probably due to the strong magnetic pinning interactions that occur between vortex screening currents and the pores. Such pinning interactions can be very effective at self- and low fields.[15]

Complicating the understanding of matters is the fact that very high self-field critical current density (J_c^{sf}) values of >5 MA/cm^2 have been reported on both vicinal and non-vicinal YBCO films[16–18] despite their supposedly different pinning structures. Since such high J_c values are more than 10% of the depairing current density (~36 MA/cm^2 at 77 K), this is very strong pinning indeed, making further improvement of J_c^{sf} quite challenging. However, recently, it has been seen that enhancement of the in-field J_c can show many more gains than are possible at self-field. For example, the studies of Macmanus-Driscoll *et al.*,[19,20] Haugan *et al.*,[21] Goyal *et al.*,[22] Miura *et al.*,[23] Gutierrez *et al.*,[24] Kim *et al.*,[25] and others have shown that the maximum pinning force can be raised from ~4 GN/m^3 for naturally grown YBCO up to ~20 GN/m^3, with barely any enhancement of J_c^{sf}. In such studies, enhanced pinning is variously attributed to pinning by point disorder (size variation[20]), insulating particles,[19,21,24] threading dislocations,[22] a combination of nanoparticles and stacking faults formed near the YBCO-substrate interface,[25] and an extensive three-dimensional (3D) network of low-T_c phases.[23] Clearly, many defects are capable of enhancing the pinning strength in YBCO thin films.

In this work, we studied the influence of growth temperature on the microstructure of YBCO films grown on 2° miscut (001) $(LaAlO_3)_{0.3}$-$(SrAl_{0.5}Ta_{0.5}O_3)_{0.7}$ (LSAT) substrates. Very high J_c^{sf} of ~5.8 MA/cm^2 at 77 K was found in a 760 °C grown film in which high densities of stacking faults, antiphase boundaries, and edge dislocations were found. However, comparison of the detailed superconducting characterizations made by us on these and various other types of YBCO films[25] and coated conductors[15,26,27] shows that such growth-generated defects can only generate about a quarter of the highest pinning forces needed to maximize the in-field properties in YBCO films containing dense arrays of second-phase nanoparticles.[23–25]

[a]Author to whom correspondence should be addressed. Electronic mail: zhijun@magnet.fsu.edu.

TABLE I. Key growth properties of the four samples. The films were grown on CeO_2 buffered LSAT substrates prepared with a 2° miscut. The CeO_2 buffer layer was nominally 20 nm thick and, like the YBCO, grown by PLD.

Sample No.	YBCO Growth temp. (°C)	YBCO Thickness (nm)	T_c (K)
1	820	255	89.9
2	790	220	89.7
3	760	210	89.5
4	730	220	89.3

II. EXPERIMENTAL DETAILS

Four YBCO films ~225 nm thick (variation of 210–255 nm) were grown by PLD on CeO_2 buffered LSAT substrates prepared with a 2° miscut. The CeO_2 buffer layer was grown with a nominal thickness of 20 nm also by PLD at 770 °C to simulate coated conductor structures.[28] The YBCO growth temperature varied in 30 °C steps from a high of 820 °C to a low of 730 °C to vary the defect density. We identify the four samples by their growth temperatures throughout this paper as shown in Table I. Bridges 100 μm wide and 500 μm long were patterned on each of the YBCO films by neodymium doped yttrium aluminum garnet laser ablation, such that the current flow was parallel to the miscut steps and the pinning force produced by defects emanating from the vicinal steps on the substrate was maximum. Four-point, small-current transport measurements of the resistivity were carried out from room temperature down to ~72 K in a Quantum Design 9 T physical property measurement system (PPMS) which enabled definition of the critical temperature T_c values at the onset of zero resistance. Transport critical current density measurements were made at 77 K at an electric field criterion of 1 μV/cm. To measure the angular dependence of J_c, the film was progressively tilted by an angle θ from the magnetic field axis, always keeping a maximum Lorentz force configuration with the current flowing perpendicular to H. To better check for thermal fluctuation depinning effects,[29] we studied the $J_c(\theta, 77\ \mathrm{K})$ properties of the 760 °C sample by milling it from 210 to 95 nm using low energy Ar ions while the sample was cooled to ~230 K.[26,30] Transmission electron microscopy (TEM) and high resolution electron microscopy (HREM) imagings were performed in a Philips CM200UT and a JEOL JEM2011. All of these observations were carried out on cross sections viewed along the current flow direction so as to show the principal pinning defects capable of resisting the Lorentz force.

III. RESULTS

A. Microstructural variation with growth temperature

Figure 1 compares cross-sectional TEM images of the YBCO-substrate interface when there is a CeO_2 buffer layer, as in most coated conductors, and when one is not present. Figure 1(a) shows the YBCO-CeO_2 interface in the 790 °C sample, while Fig. 1(b) shows the YBCO-LSAT interface in a film grown at 850 °C. Without CeO_2, the step height at the miscut is only ~1 nm, almost the same as the c-axis parameter of YBCO, while with CeO_2, the step height is tripled to ~3 nm, propagating defects deep into the YBCO layer.

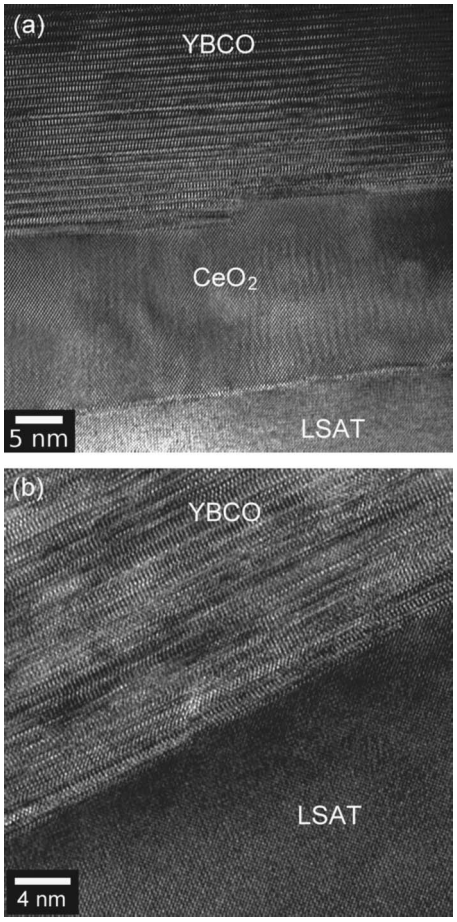

FIG. 1. TEM images showing the interfaces between the YBCO layer and (a) the CeO_2 buffer layer on LSAT of sample 2 and (b) the bare LSAT substrate of on 850 °C grown sample. With CeO_2, the step height is ~3 nm, which is three times greater than that on bare LSAT substrates.

Figures 2(a)–2(c) present cross-sectional TEM images of the YBCO films grown at 790, 760, and 730 °C, respectively. They demonstrate that lower growth temperatures produce significantly greater defect densities. Figure 2(a) shows that stacking faults in the *ab* plane are the most obvious defects in the 790 °C film and they are always more frequent near the YBCO-CeO_2 interface. The stacking faults are no longer seen in the upper layer of the 790 °C film, which has a relatively clean and continuous YBCO microstructure. In the 760 °C film, as shown in Fig. 2(b), the dominant defects are antiphase boundaries and stacking faults, as already noted in a study of YBCO films grown on vicinal $SrTiO_3$ substrates at 750 °C by Haage *et al.*[9] The high density antiphase boundaries, partially highlighted with solid black lines, originate from the vicinal steps on the LSAT. They propagate imperfectly through the CeO_2 and then meander through the YBCO thickness, generating a complex defect network. The defect microstructure of the 730 °C film is very similar to that of the 760 °C film but on a significantly finer scale, as shown in Fig. 2(c). However, as shown in the inset of Fig. 2(c), it also contains *a*-axis grains, which may significantly obstruct the current-carrying cross section. Such *a*-axis grains are very common in YBCO grown at lower growth temperatures.[31,32]

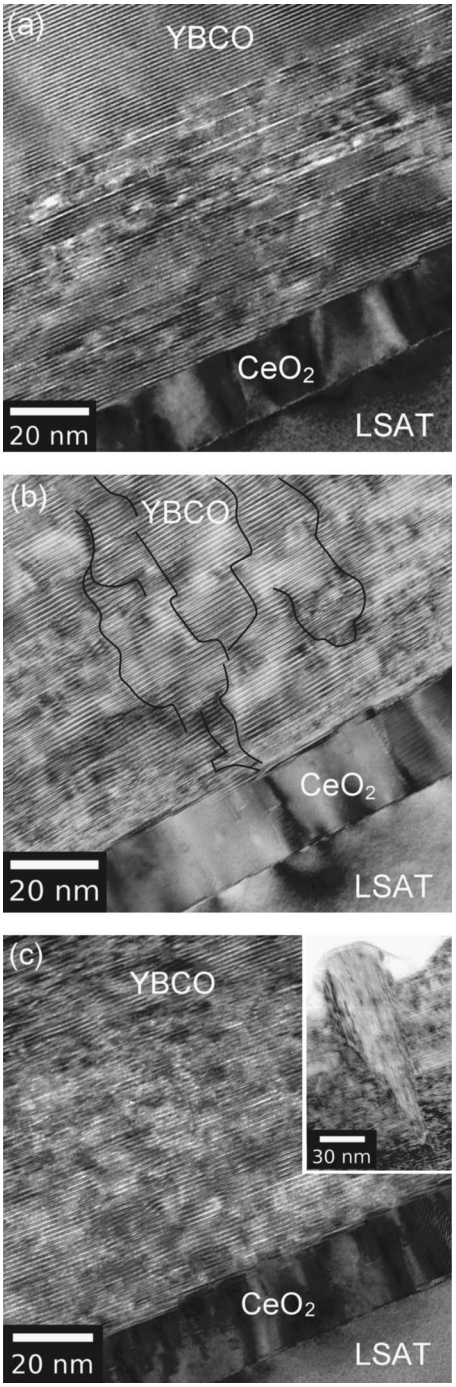

FIG. 2. Cross-sectional TEM images of the samples grown at various temperatures of (a) 790 °C, (b) 760 °C, and (c) 730 °C. (a) Stacking faults (white line contrasts) are seen near the YBCO-CeO_2 interface but not in the upper layer of YBCO. (b) Black lines highlight a high density of highly meandered antiphase boundaries, which are the dominant defect structure. (c) The defect microstructure is very similar to that of (b) but on a significantly finer scale. Inset of (c): *a*-axis grains are present near the top layer of YBCO.

Figure 3 is a HREM image from the 760 °C grown film taken near the YBCO-CeO_2 interface. It shows that the antiphase boundaries lie not only along the *c* axis but also in the *ab* plane. They are usually terminated by edge dislocations lying in the *ab* planes, as marked by the edge dislocation symbols. Stacking faults are the second major defect type visible from Fig. 3, marked by black dashed lines. They

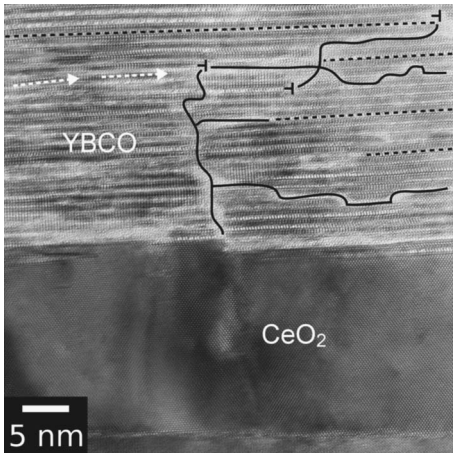

FIG. 3. HREM image near the YBCO-CeO_2 interface on the 760 °C grown sample shows that antiphase boundaries (solid black lines) are originated from the edge of the miscut step and are often terminated by edge dislocations. Stacking faults are also seen, marked as black dashed lines. The white dashed arrows present the tilting of *ab* planes.

are uniformly distributed through thickness along *ab* planes. Figure 3 also shows that the antiphase boundaries appear as broad white contrasts because the boundary planes are not perfectly normal to the imaging plane. Following the irregular terraces of the CeO_2, the YBCO tends to break into small domains with small out-of-plane mosaic spreads. The *ab* planes are highlighted with white dashed arrows, from which it can be seen that the *ab* planes are not straight but tilted as much as 2°–5° from the substrate. This *ab* plane tilting causes an angular dispersion of the stacking faults and antiphase boundaries about the nominal film plane direction, which can produce an irregular angular dependence of J_c in magnetic fields,[33,34] as will also appear in Fig. 5.

B. Change of superconducting properties with growth temperature

Figure 4 shows the field dependence of J_c at 77 K for all four YBCO films. There is a clear dependence of J_c^{sf} on the YBCO growth temperature: J_c^{sf} increases from 2.8 to 3.7 to 5.8 MA/cm^2 with decreasing growth temperature from 820 to 760 °C but then decreases to 3.8 MA/cm^2 at 730 °C, as illustrated in the inset of Fig. 4. The maximum J_c^{sf} is ~5.8 MA/cm^2 from the 760 °C film, for which the

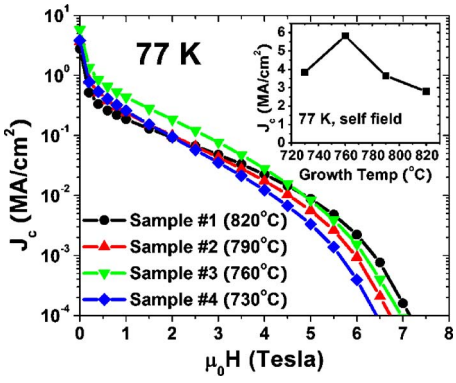

FIG. 4. (Color online) Field dependence of J_c at 77 K for all four YBCO films. The inset shows the dependence of J_c^{sf} on the film growth temperature.

TABLE II. Summary of the superconducting properties at 77 K of all four samples. H_{max} is where the maximum F_p was found.

Sample	J_c^{sf} (MA/cm^2)	J_c(1 T) (MA/cm^2)	J_c(4 T) (MA/cm^2)	H_{irr} (T)	F_p^{max} (GN/m^3)	H_{max} (T)
1, 820 °C	2.79	0.186	0.0224	7.1	1.9	1.5
2, 790 °C	3.65	0.241	0.0176	6.7	2.4	1
3, 760 °C	5.81	0.436	0.0279	7	4.4	1
4, 730 °C	3.83	0.257	0.0123	6.4	2.6	0.8

in-field J_c is also the best in applied magnetic fields $H < 4$ T. For all the samples, the irreversibility field H_{irr}, defined at $J_c = 100$ A/cm^2, varies only from 6.5 to 7.1 T, championed by the highest growth temperature film (820 °C) rather than the highest J_c^{sf} film (760 °C). Above ~4 T, the ranking of J_c correlates well to the highest value of H_{irr}. The superconducting properties of the four samples are summarized in Table II.

The angular dependence of J_c, $J_c(\theta)$, at 1 T for all four films is shown in Fig. 5. Because of the miscut and its consequent *ab*-plane tilting, the shape of the $J_c(\theta)$ curves is not symmetric about the film surface ($\theta = 180°$). This asymmetry grows strongly as the growth temperature decreases from 820 to 760 °C. The sharp drop of J_c from $\theta = 180°$ to 170° for the 760 °C sample is probably due to vortex channeling.[35] Despite the asymmetric and dissimilar shapes of the $J_c(\theta)$ curves, the magnitude of J_c(77 K, 1 T) is improved in all directions with decreasing growth temperature, reaching a maximum at 760 °C before again decreasing at 730 °C.

Figure 6 presents the bulk flux pinning force curves for fields normal to the film plane, which clearly discriminate between the four films. The magnitude of F_p^{max} follows the same tendency as the J_c^{sf} values when the growth temperature decreases from 820 to 730 °C. The best value of F_p^{max} ~4.4 GN/m^3 is found at 1 T in the 760 °C film, more than twice the ~1.9 GN/m^3 value found in the 820 °C grown film. There is a tendency for the field at which the maximum pinning force occurs to rise monotonically from ~0.9 T for the 730 °C film to ~1.5 T for the 820 °C film.

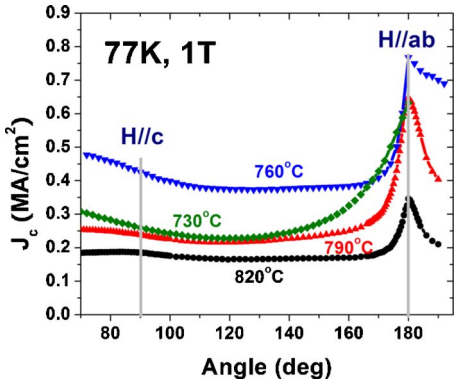

FIG. 5. (Color online) Angular dependence of J_c at 77 K, 1 T for all four films. The curves appear asymmetric because of the miscut. In general, J_c is increased in all directions as the growth temperature decreases down to 760 °C.

IV. DISCUSSION

The pinning effects of substrate-induced dislocations are well documented.[3,4] Indeed, the enhancement of J_c^{sf} from ~10^3 A/cm^2 for YBCO single crystals to >5 MA/cm^2 for epitaxial YBCO thin films makes it clear that thin-film growth defects are very effective pinning centers. The vicinal YBCO films studied in this work have a maximum J_c^{sf} of 5.8 MA/cm^2, indicating a similarly good vortex pinning nanostructure. We thus believe that these four films are representative of the pinning effects of naturally generated defects, especially since we have used 2° vicinal LSAT substrates with a CeO_2 buffer layer to enhance their defect-generating effects.

From the TEM images in Fig. 2, it is clear that decreasing the growth temperature systematically increases the defect density, which correlates well to the increase of J_c^{sf} from 2.8 to 5.8 MA/cm^2 and of F_p^{max} from 1.9 to 4.4 GN/m^3 down to 760 °C. Indeed, studies of the angular dependence (Fig. 5) at 77 K, 1 T show that strong-pinning effects develop over a broader angular range as the temperature is lowered, and even that the J_c of the 730 °C film can be highest in a small angular range of θ (165°–175°). This is a strong sign that the real vortex pinning is continuously enhanced as the growth temperature decreases down to 730 °C even though the presence of current-blocking *a*-axis grains results in a significant underestimate of the vortex pinning J_c since the local J_c is certainly significantly higher than the value defined by I_c/A, where I_c is the critical current and A is the total cross section of YBCO. However, instead of show-

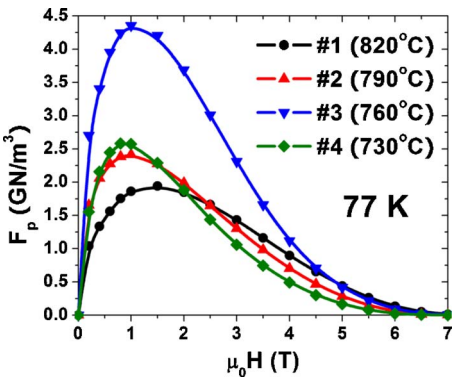

FIG. 6. (Color online) The bulk flux pinning force curves for all four films for fields normal to the film plane. The magnitude of F_p^{max} follows the same tendency as the J_c^{sf} values when the growth temperature decreases from 820 to 730 °C. As noted in the discussion, we believe that current blocking by *a*-axis grains significantly depresses the magnitude of F_p for the 730 °C curve.

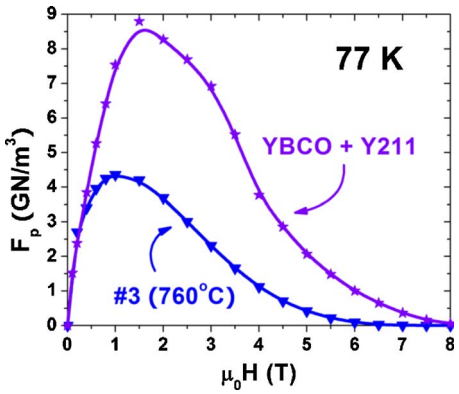

FIG. 7. (Color online) A comparison of the pinning force curves for the best present sample (760 °C) with a recent PLD YBCO film made with ~5 vol % of strong-pinning Y_2BaCuO_5 (Y211) nanoprecipitates (Ref. 25).

ing a uniform improvement of J_c at all fields, the high densities of antiphase boundaries, stacking faults, and edge dislocations manifest themselves in the enhanced J_c performance only in the low-field range ($H<4$ T). Above 4 T, J_c of the 760 °C grown film (highest J_c^{sf}) simply does not benefit from its higher defect densities in comparison to the 820 °C grown film, which has no discernible pinning defects in the TEM images (not shown here) and has the smallest J_c^{sf} value of 2.8 MA/cm^2. Thus, we conclude that these growth and substrate-induced defects, although capable of greatly enhancing J_c^{sf}, are not strong-pinning centers at higher fields, as also noted by the insensitivity of H_{irr} to the film growth temperature.

The H_{irr} values are all ~7 T, a value common for high quality PLD YBCO films[15,36] but one which does not reflect the enhancements seen in several recent studies of the effect of nanoparticles and other precipitations. Such improved pinning samples have produced H_{irr} values of >9 T at 77 K.[19,21,22,24,37] Figure 7 compares the pinning force curve for the best present sample (760 °C) with a recent PLD YBCO film made with ~5 vol % of strong-pinning Y_2BaCuO_5 (Y211) nanoprecipitates.[25] The latter has approximately twice the F_p value over the whole field range, its F_p^{max} being 8.8 GN/m^3, although actually J_c^{sf} was only 3.4 MA/cm^2. The distinctly inferior F_p values of the best present samples grown at 760 °C suggests that there is still plenty room for improving the pinning strength but that the route to doing this is by incorporating nanoparticles that can provide strong vortex core pinning.

Besides the magnitude of F_p, the position of the maximum in F_p also matters. For magnetic field applications, e.g., superconducting motors or rotating machines, their operating fields are typically 1–3 T,[38,39] making it desirable that F_p^{max} falls in the middle of this region, too. Obviously, even the best of the present samples does not satisfy this requirement because F_p^{max} peaks at ~1 T, then quickly decreases. To shift the F_p curve upward and to higher fields requires denser and stronger pinning interactions that can improve J_c in medium and high fields. We thus conclude that natural growth defects in YBCO, though clearly strong pinning at low fields, are not by themselves capable of optimizing pinning in YBCO films.

The suboptimum *c*-axis in-field pinning efficiency of antiphase boundaries, stacking faults, and edge dislocations can be understood from their geometries. The stacking faults and edge dislocations, although having high densities, are mostly parallel to the film surface. They are therefore unfavorable for pinning vortices parallel to the *c*-axis. Planar antiphase boundaries are well defined pinning sites due to the suppression of superconducting order parameter along the boundary plane,[40,41] but their pinning strength strongly decreases with increasing field.[40] This fact is quite understandable, considering that their effective thickness, including strain field around the antiphase boundary plane, is only ~1–2 nm according to our TEM observation, which is much smaller than the coherence length of YBCO [~4 nm at 77 K (Ref. 42)]. So, the antiphase boundary cannot accommodate the whole vortex core, and unlike many strong nonsuperconducting second-phase pinning centers[21,26] in YBCO, the antiphase boundaries are not completely insulating, which makes them less effective pinning centers. Thus, some random fluctuation of the Lorentz force at high magnetic fields may cause the vortices to move within or slightly perpendicular to the antiphase boundary planes, generating dissipative voltage. At high fields where the pinning potential is strongly reduced, thermal fluctuation depinning[29] may become easy.

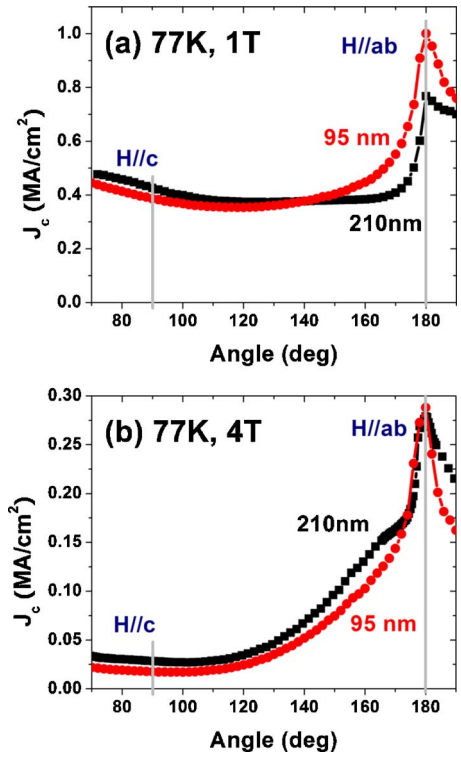

FIG. 8. (Color online) $J_c(\theta,77\ \mathrm{K})$ as a function of film thickness at (a) 1 T and (b) 4 T for the 760 °C grown film.

To check the influence of thermal fluctuation depinning effects, we Ar ion milled the 760 °C film from 210 to 95 nm thickness. Figures 8(a) and 8(b) present $J_c(\theta,77\ \mathrm{K})$ as a function of film thickness at 1 and 4 T, respectively. At 1 T, where F_p^{max} occurs, J_c slightly decreases near the *c*-axis peak but is significantly improved for all other directions and remains asymmetric, consistent with strong-pinning interactions between vortices and the vicinally generated defects at both 210 and 95 nm thicknesses. It appears in fact that ther-

mal fluctuation depinning starts to occur at 1 T when H is close to the c-axis, but since J_c becomes higher for θ more than about 50° from the c-axis, thermal fluctuation effects cannot then control J_c. By contrast, at 4 T (well above $F_p^{\max}$) $J_c(\theta,95\ \text{nm})$ is always smaller than $J_c(\theta,210\ \text{nm})$ for all θ, and the extra vicinal hump at ~170° for $J_c(\theta,4\ \text{T},210\ \text{nm})$ is no longer visible in its 95 nm counterpart. This behavior is consistent with thermal fluctuations exciting vortices out of the vicinal defects when the film is very thin and in high fields. The thickness dependence of $J_c(\theta)$ at 4 T strongly resembles a parallel study of ours on an 850 °C grown film with low defect density and low J_c^{sf} where we found very strong evidence for thermal fluctuation depression of J_c in thinner films.[12] In this study, a significant decrease of J_c in all directions at all fields was found when thinned films were compared to their full-thickness values.[12,43] Milling the films also wiped out the asymmetric features of the $J_c(\theta)$ curve, such as the c-axis correlated peak and humps near the ab-plane peak produced by the substrate miscut. In sharp contrast, YBCO films with strong 3D pinning centers showed in-field $J_c(\theta)$ behavior which was insensitive to thickness.[26] Summarizing, the present data show that antiphase boundaries, stacking faults, and edge dislocations are effective vortex pinning centers only at low fields, leaving higher field properties above $\sim 1/2H_{\text{irr}}$ strongly compromised by thermal fluctuation depinning effects.

The route to better performance in the high magnetic field region has in fact been clearly indicated in many recent studies, even if a full field characterization is not presented in each case. Examples include YBCO films with $BaZrO_3$ nanoparticle additions,[19,24] multilayer YBCO films with Y211 interlayers,[21,25] etc. In most cases, J_c was found to be improved at all fields up to H_{irr}, which sometimes is also significantly enhanced.[25,26] $F_p^{\max}$ values are also enhanced to values $>8\ \text{GN/m}^3$, which peak at ~2 T or higher. We should, however, note that the combination of Y211 nanoparticles growing in dense stacking faults near the substrate interface in the recent study of Kim *et al.*[25] raised $F_p^{\max}$ to $14\ \text{GN/m}^3$, showing that the combined effects of both structural and insulating pins can be very effective. However, the most spectacular is that $F_p^{\max}$ values reach $20\ \text{GN/m}^3$, five times higher than the best present sample.[23,24] We attribute the stronger pinning of such films to both stronger elementary pinning interactions between the vortex cores and insulting particles of Y211 and $BaZrO_3$, and to optimization of the size and density of the precipitate distributions. The case of the Sm-rich low-temperature grown films of SmBCO (Ref. 23) is interesting because $20\ \text{GN/m}^3$ is attained by a low-T_c phase, somewhat reminiscent of the proximity-coupled pinning that occurs in optimized Nb–Ti.[44] Thus, YBCO seems to offer the special capability of both being able to incorporate insulating particles with strong-pinning interactions that perhaps peak at volume fractions of ~10% or lower, or accept weakly superconducting pins of much higher volume fraction that are also spectacularly strong-pinning centers. To attain such properties in the most suitable fashion for the many individual ways in which YBCO is presently made today, whether by *in situ* methods such as PLD, metal organic chemical vapor deposition, or electron-beam evaporation, or by *ex situ* methods such as the BaF_2 route or metal organic deposition (MOD), means that many types of strategy for maximizing J_c may be employed. One message of the present study is that attention to the in-field pinning performance rather than to J_c^{sf} or the low-field α pinning parameter[45] will be important to maximize the pinning efficiency of YBCO.

V. CONCLUSIONS

By varying the growth temperature of PLD YBCO films, we find pinning properties enhanced by decreasing the growth temperature to 760 °C, which achieves $J_c^{\text{sf}}(77\ \text{K})$ and $F_p^{\max}$ values of $\sim 5.8\ \text{MA/cm}^2$ and $\sim 4.4\ \text{GN/m}^3$, respectively. TEM imaging found a high density of antiphase boundary, stacking fault, and edge dislocation pinning defects, which are believed to be responsible for the enhanced J_c^{sf} and $F_p^{\max}$. However, the in-field J_c results suggest that the defect structures mentioned above are not strong enough to be effective pins at high fields. We conclude that naturally generated defects are not the ultimate solution for industrial applications, and that the self-field J_c is not the best measure of the flux pinning efficiency.

ACKNOWLEDGMENTS

This work was supported by AFOSR under Grant Nos. FA9550-06-1-0415 and F49620-01-1-0464. JEOL JEM2011 purchased by NSF Grant No. DMR-9625692 is maintained and supported by NHMFL, which is supported by the NSF under Cooperative Agreement No. DMR-0084173 and the State of Florida.

[1] L. Civale, A. D. Marwick, M. W. Mcelfresh, T. K. Worthington, A. P. Malozemoff, F. H. Holtzberg, J. R. Thompson, and M. A. Kirk, Phys. Rev. Lett. **65**, 1164 (1990).
[2] J. Mannhart, D. Anselmetti, J. G. Bednorz, A. Catana, C. Gerber, K. A. Muller, and D. G. Schlom, Z. Phys. B: Condens. Matter **86**, 177 (1992).
[3] H. Wang, S. R. Foltyn, P. N. Arendt, Q. X. Jia, and X. Zhang, Physica C **444**, 1 (2006).
[4] B. Dam, J. M. Huijbregtse, F. C. Klaassen, R. C. F. van der Geest, G. Doornbos, J. H. Rector, A. M. Testa, S. Freisem, J. C. Martinez, B. Stauble-Pumpin, and R. Griessen, Nature (London) **399**, 439 (1999).
[5] J. M. Huijbregtse, B. Dam, R. C. F. van der Geest, F. C. Klaassen, R. Elberse, J. H. Rector, and R. Griessen, Phys. Rev. B **62**, 1338 (2000).
[6] B. L. Low, S. Y. Xu, C. K. Ong, X. B. Wang, and Z. X. Shen, Supercond. Sci. Technol. **10**, 41 (1997).
[7] B. Dam, J. H. Rector, J. M. Huijbregtse, and R. Griessen, Physica C **305**, 1 (1998).
[8] D. H. Lowndes, X. Y. Zheng, S. Zhu, J. D. Budai, and R. J. Warmack, Appl. Phys. Lett. **61**, 852 (1992).
[9] T. Haage, J. Zegenhagen, J. Q. Li, H. U. Habermeier, M. Cardona, C. Jooss, R. Warthmann, A. Forkl, and H. Kronmuller, Phys. Rev. B **56**, 8404 (1997).
[10] L. Mechin, P. Berghuis, and J. E. Evetts, Physica C **302**, 102 (1998).
[11] S. Y. Xu, C. K. Ong, and X. Zhang, Solid State Commun. **107**, 273 (1998).
[12] S. I. Kim, Z. Chen, F. Kametani, K. J. Choi, C. B. Eom, A. Gurevich, and D. C. Larbalestier (unpublished).
[13] T. J. Jackson, J. S. Abell, R. Chakalov, M. S. Colclough, C. N. W. Darlington, I. P. Jones, G. Kong, C. M. Muirhead, and F. Wellhofer, Thin Solid Films **468**, 332 (2004).
[14] R. L. S. Emergo, J. Z. Wu, T. J. Haugan, and P. N. Barnes, Appl. Phys. Lett. **87**, 232503 (2005).
[15] S. I. Kim, A. Gurevich, X. Song, X. Li, W. Zhang, T. Kodenkandath, M. W. Rupich, T. G. Holesinger, and D. C. Larbalestier, Supercond. Sci. Technol. **19**, 968 (2006).
[16] S. R. Foltyn, P. Tiwari, R. C. Dye, M. Q. Le, and X. D. Wu, Appl. Phys.

Lett. **63**, 1848 (1993).
[17]S. R. Foltyn, H. Wang, L. Civale, Q. X. Jia, P. N. Arendt, B. Maiorov, Y. Li, M. P. Maley, and J. L. MacManus-Driscoll, Appl. Phys. Lett. **87**, 162505 (2005).
[18]F. J. Baca, D. Fisher, R. L. S. Emergo, and J. Z. Wu, Supercond. Sci. Technol. **20**, 554 (2007).
[19]J. L. Macmanus-Driscoll, S. R. Foltyn, Q. X. Jia, H. Wang, A. Serquis, L. Civale, B. Maiorov, M. E. Hawley, M. P. Maley, and D. E. Peterson, Nat. Mater. **3**, 439 (2004).
[20]J. L. MacManus-Driscoll, S. R. Foltyn, Q. X. Jia, H. Wang, A. Serquis, B. Maiorov, L. Civale, Y. Lin, M. E. Hawley, M. P. Maley, and D. E. Peterson, Appl. Phys. Lett. **84**, 5329 (2004).
[21]T. Haugan, P. N. Barnes, R. Wheeler, F. Meisenkothen, and M. Sumption, Nature (London) **430**, 867 (2004).
[22]A. Goyal, S. Kang, K. J. Leonard, P. M. Martin, A. A. Gapud, M. Varela, M. Paranthaman, A. O. Ijaduola, E. D. Specht, J. R. Thompson, D. K. Christen, S. J. Pennycook, and F. A. List, Supercond. Sci. Technol. **18**, 1533 (2005).
[23]M. Miura, Y. Ichino, Y. Yoshida, Y. Takai, K. Matsumoto, A. Ichinose, S. Horii, and M. Mukaida, Physica C **445**, 643 (2006).
[24]J. Gutierrez, A. Llordes, J. Gazquez, M. Gibert, N. Roma, S. Ricart, A. Pomar, F. Sandiumenge, N. Mestres, T. Puig, and X. Obradors, Nat. Mater. **6**, 367 (2007).
[25]S. I. Kim, F. Kametani, Z. Chen, A. Gurevich, D. Larbalestier, T. Haugan, and P. Barnes, Appl. Phys. Lett. **90**, 252502 (2007).
[26]Z. Chen, D. M. Feldmann, X. Song, S. I. Kim, A. Gurevich, J. L. Reeves, Y. Y. Xie, V. Selvamanickam, and D. C. Larbalestier, Supercond. Sci. Technol. **20**, S205 (2007).
[27]Z. Chen, D. M. Feldmann, D. Larbalestier, T. Holesinger, X. Li, W. Zhang, and M. Rupich, Appl. Phys. Lett. **91**, 052508 (2007).
[28]M. P. Paranthaman, S. Sathyamurthy, M. S. Bhuiyan, A. Goyal, T. Kodenkandath, X. Li, W. Zhang, C. L. H. Thieme, U. Schoop, D. T. Verebelyi, and M. W. Rupich, IEEE Trans. Appl. Supercond. **15**, 2632 (2005).
[29]A. Gurevich, Supercond. Sci. Technol. **20**, S128 (2007).
[30]D. M. Feldmann, D. C. Larbalestier, R. Feenstra, A. A. Gapud, J. D. Budai, T. G. Holesinger, and P. N. Arendt, Appl. Phys. Lett. **83**, 3951 (2003).
[31]R. K. Singh and D. Kumar, Mater. Sci. Eng., R. **22**, 113 (1998).
[32]F. Goerke and A. Thorns, Physica C **251**, 247 (1995).
[33]D. H. Lowndes, D. K. Christen, C. E. Klabunde, Z. L. Wang, D. M. Kroeger, J. D. Budai, S. Zhu, and D. P. Norton, Phys. Rev. Lett. **74**, 2355 (1995).
[34]B. Maiorov, B. J. Gibbons, S. Kreiskott, V. Matias, T. G. Holesinger, and L. Civale, Appl. Phys. Lett. **86**, 02504 (2005).
[35]J. H. Durrell, G. Burnell, V. N. Tsaneva, Z. H. Barber, M. G. Blamire, and J. E. Evetts, Phys. Rev. B **70**, 214508 (2004).
[36]T. Matsushita, M. Kiuchi, K. Kimura, S. Miyata, A. Ibi, T. Muroga, Y. Yamada, and Y. Shiohara, Supercond. Sci. Technol. **18**, S227 (2005).
[37]K. Matsumoto, T. Horide, A. Ichinose, S. Horii, Y. Yoshida, and M. Mukaida, Jpn. J. Appl. Phys., Part 2 **44**, L246 (2005).
[38]S. S. Kalsi, K. Weeber, H. Takesue, C. Lewis, H. W. Neumueller, and R. D. Blaugher, Proc. IEEE **92**, 1688 (2004).
[39]D. Larbalestier, A. Gurevich, D. M. Feldmann, and A. Polyanskii, Nature (London) **414**, 368 (2001).
[40]C. Jooss, R. Warthmann, and H. Kronmuller, Phys. Rev. B **61**, 12433 (2000).
[41]C. Jooss, R. Warthmann, H. Kronmuller, T. Haage, H. U. Habermeier, and J. Zegenhagen, Phys. Rev. Lett. **82**, 632 (1999).
[42]G. Blatter, M. V. Feigelman, V. B. Geshkenbein, A. I. Larkin, and V. M. Vinokur, Rev. Mod. Phys. **66**, 1125 (1994).
[43]D. C. Larbalestier, presented at the Superconductivity for Electric System 2005 Annual Peer Review, Washington, DC, 2005 (unpublished).
[44]C. Meingast and D. C. Larbalestier, J. Appl. Phys. **66**, 5971 (1989).
[45]L. Civale, B. Maiorov, A. Serquis, J. O. Willis, J. Y. Coulter, H. Wang, Q. X. Jia, P. N. Arendt, M. Jaime, J. L. MacManus-Driscoll, M. P. Maley, and S. R. Foltyn, J. Low Temp. Phys. **135**, 87 (2004).